## Supporting Information

# Coordination of the copper centers in particulate methane monooxygenase: comparison between methanotrophs and characterization of the $Cu_C$ site by EPR and ENDOR spectroscopies

Richard J. Jodts, Matthew O. Ross[$], Christopher W. Koo, Peter E. Doan Amy C. Rosenzweig*, and Brian M. Hoffman*

*Departments of Chemistry and Molecular Biosciences, Northwestern University, Evanston, Illinois 60208*
*[$]Present Address: Department of Chemistry, University of Chicago, Chicago, Illinois 60637*

*Email: amyr@northwestern.edu, bmh@northwestern.edu

## Supporting Methods

### Preparation of $[Cu(NH_3)_4]^{2+}$

$Cu(NH_3)_4^{2+}$ was prepared in MilliQ water by adding 1 M NaOH to a solution of ~25 mM $NH_4Cl$ and 2 mM $Cu(II)Cl_2$ until the pH was ~9 and the solution turned a deep blue color. A small aliquot was diluted to ~1 mM with a mixture of ethylene glycol and water.

**DFT Calculations for $[Cu(NH_3)_4]^{2+}$** All density functional theory (DFT) calculations were carried out in ORCA 4.2.1.[1] Starting geometry for the copper complex was created in situ using Avogadro.[2] Geometry and single point energy calculations utilized spin unrestricted B3LYP/G hybrid functional set[3-4] and Ahlrichs' valence triple-ξ with a polarization function basis set.[5] For the proton hyperfine calculations Barone's EPR-III basis set[6-7] was used, while the Cu(II) atom utilized Kutzelnigg's basis set (IGLO-III);[8] B3LYP/G was again used as the functional set in combination with the accurate spin−orbit coupling operator [RI-SOMF(1X)].[9]

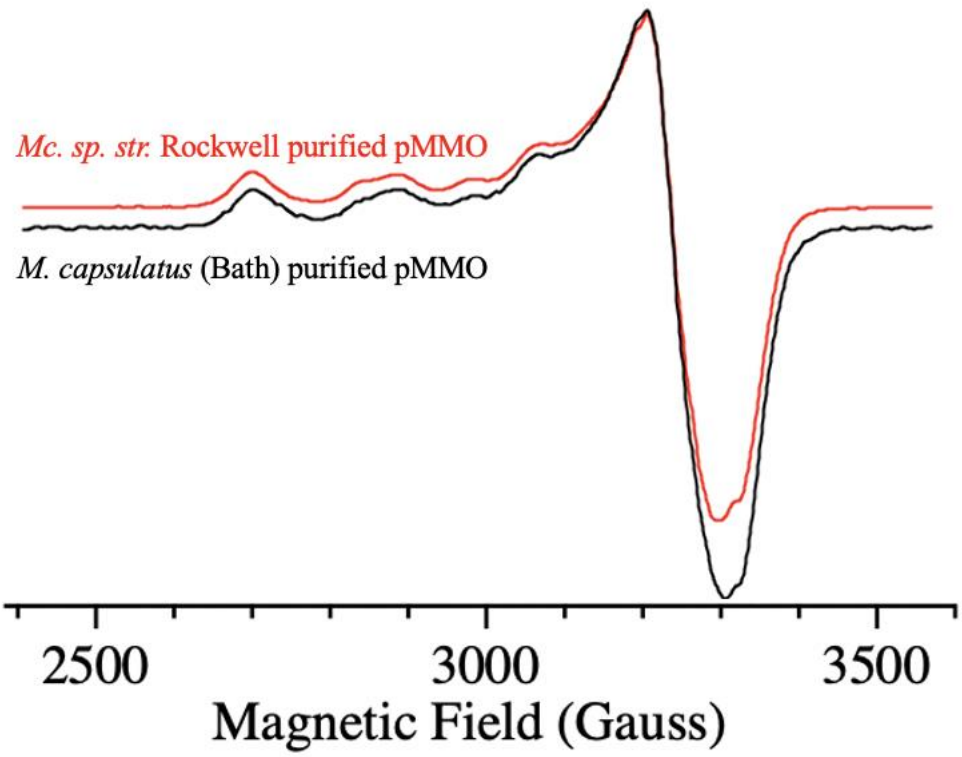


**Figure S1.** Overlay of X-band EPR spectra of purified *Mc.* sp. str. Rockwell (red) and *M. capsulatus* (Bath) pMMOs. The spectra are identical in terms of g and $^{63}$Cu $A_{\|}$ values, the most definitive features for Cu(II) EPR. *Conditions:* 9.37 GHz, 20 K, 12.5 G modulation, 320 ms time constant, 200 µW MW power. The spectra were collected on the same day for accurate comparison.

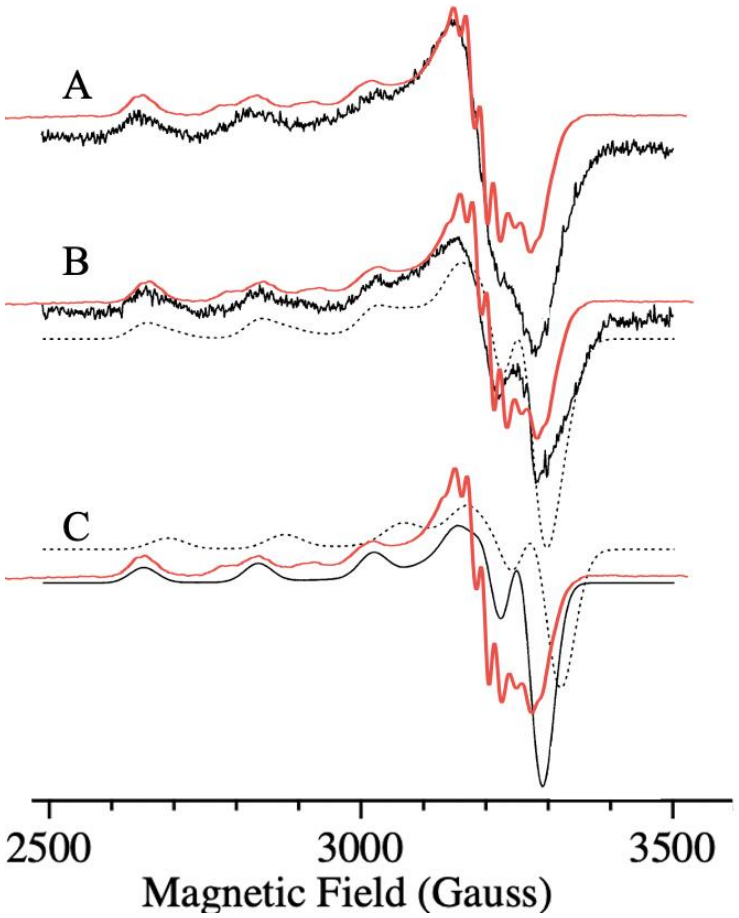


**Figure S2.** Overlay of X-band EPR spectrum of purified *Mc.* sp. str. Rockwell pMMO presented in this paper (red, from **Figure 2C** main text) with the three previously reported EPR spectra of type II *Mc.* sp. str. M pMMO[10] (black), including (A) membrane-bound pMMO (B) solubilized pMMO, and (C) simulations of the two Cu(II) signals observed in (C) from ref. 10. The overlay of the *Mc.* sp. str. Rockwell spectrum (red) shows that the $Cu_C$ site was not observed in the type II pMMOs in previous samples. Its absence may be due to not adding copper to the lysis buffer. As shown in Figure S4, this leads to only $Cu_B$ being observed by EPR for *Mc.* sp. str. Rockwell pMMO. It is possible that there is some underlying $Cu_C$ signal in (B), as evident by $\mathbf{g}_\perp$, but due to the resolution, it is not obvious. *Conditions* are reported in ref. 10, with those for the red trace in the main text.

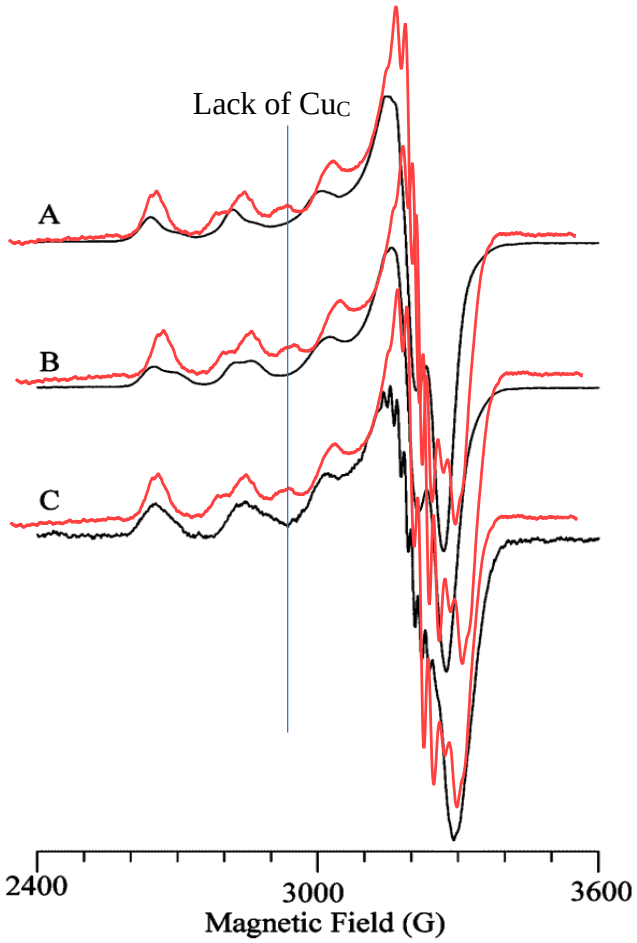


**Figure S3.** Overlay of purified *Mc.* sp. str. Rockwell pMMO X-band EPR spectrum presented in this paper (red, **Figure 2C** main text) with the three previously reported EPR spectra of type II *Methylosinus trichosporium* OB3b pMMO[11] (black), including (A) membrane-bound pMMO, (B) solubilized pMMO, and (C) purified pMMO The Cu(II) spectra in (A) and (B) are not related to pMMO since the g|| and the $^{63/65}$Cu A|| do not match those of the Cu$_B$ or Cu$_C$ site. The purified pMMO spectrum appears to only have the Cu$_B$ site. The lack of the Cu$_C$ site in the purified pMMO spectrum is evident by the lack of the +1/2 hyperfine line, as shown with the blue vertical line. *Conditions* of black are described in the referece, red is described in text.

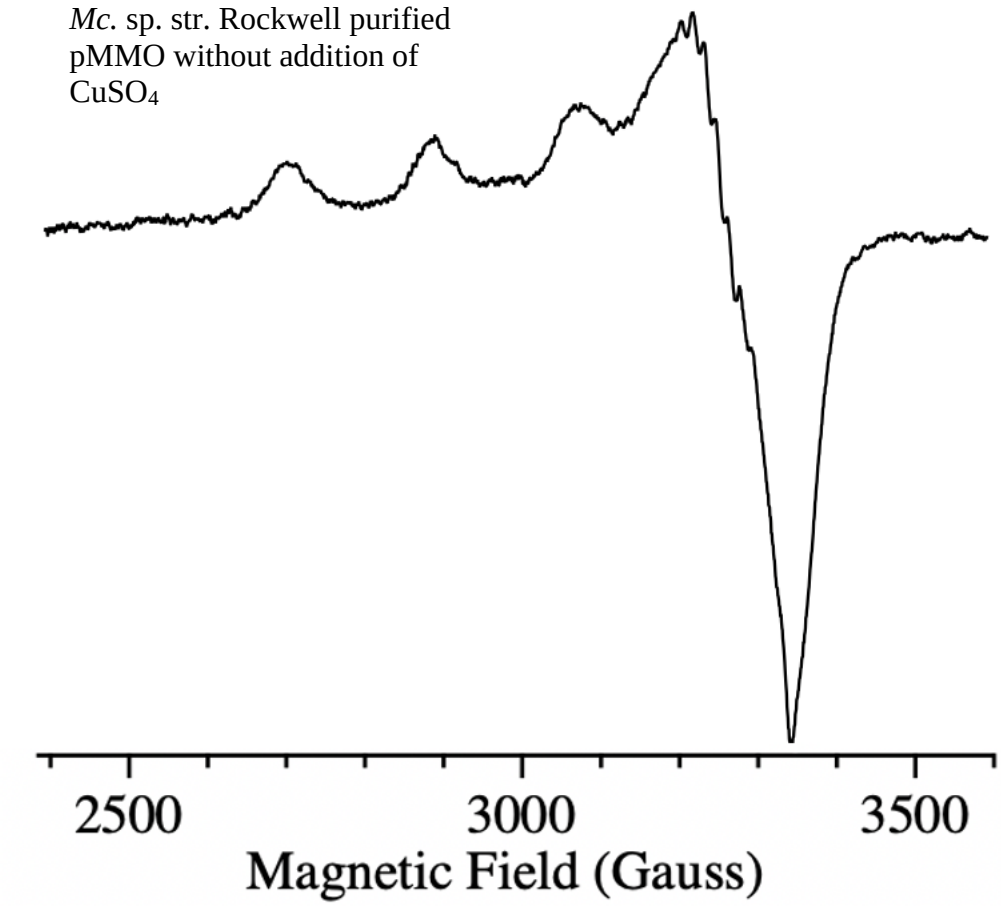


**Figure S4.** X -Band EPR spectrum of *Mc.* sp. str. Rockwell purified pMMO without the addition of $CuSO_4$ at lysis. The spectrum exhibits only the $Cu_B$ signal, and is identical to that of *Mc.* sp. str. Rockwell whole cells (**Figure 2A**) and purified/reduced *Mc.* sp. str. Rockwell pMMO (**Figure 2D**), with no $Cu_C$ signal. These samples do not have methane oxidation activity. *Conditions:* 77K, 12.5 G modulation, 10G/s sweep rate, 320 ms time constant, 200μW MW power, 9.34 GHz MW frequency.

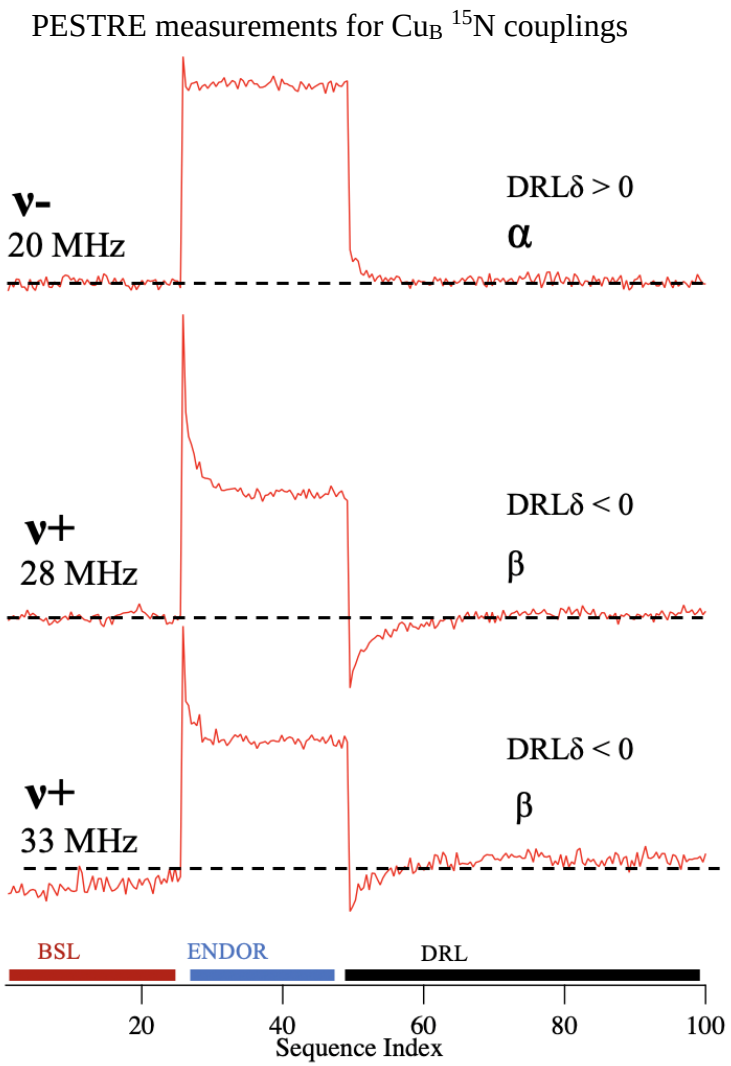


**Figure S5.** PESTRE measurements for sign determination of the strongly coupled $Cu_B$ $^{15}N$ in *Mc.* sp. str. Rockwell in vivo pMMO. The couplings were found to be negative in sign for both peaks shown in **Figure 3**. *Conditions:* 34.77 GHz, 100 ms repetition time, $\pi$ = 120 ns, $\tau$ = 600 ns, TRF = 15 μs, RF tail = 5 μs, 25 shots, 24 off.

PESTRE measurements for $Cu_B$ $^1H$ couplings

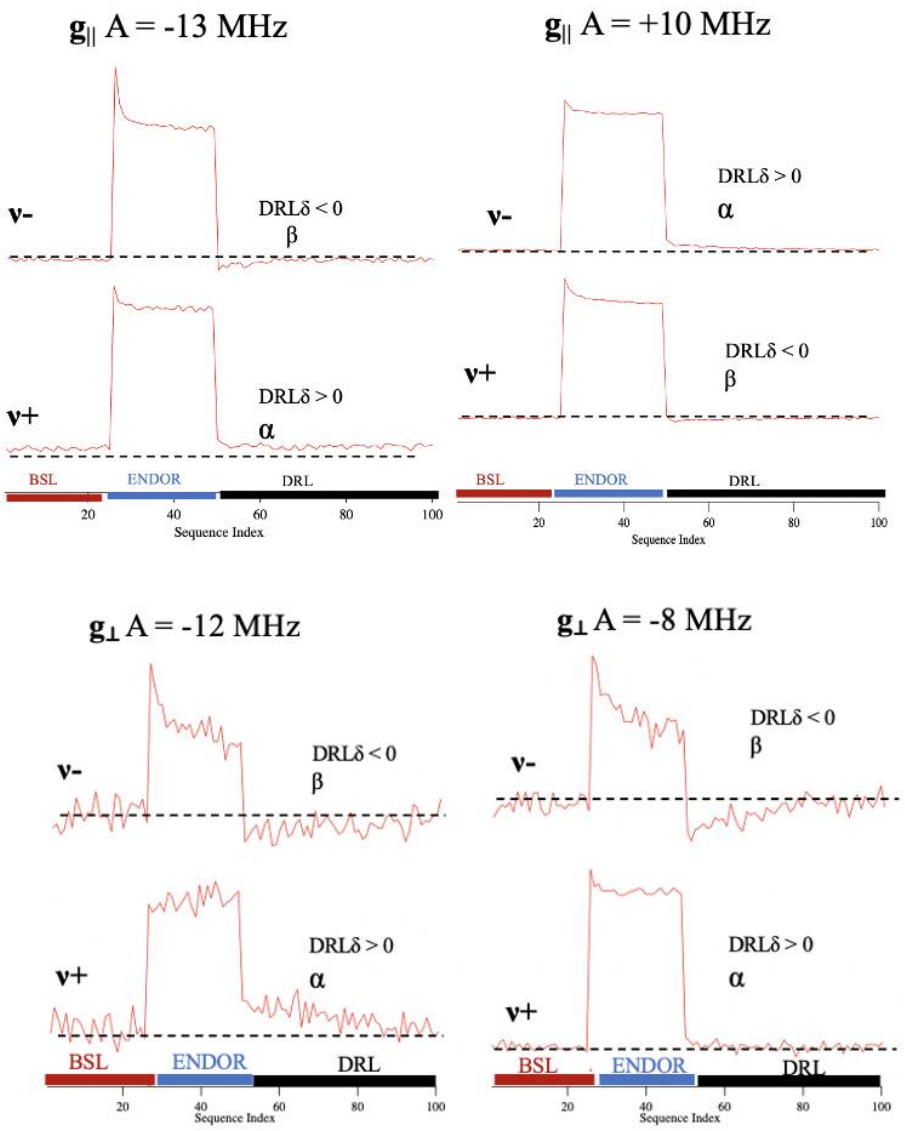


**Figure S6.** PESTRE measurements on the large couplings of in vivo *Mc.* sp. str. Rockwell pMMO ($Cu_B$ site) as resolved from the stochastic $^1H$ ENDOR experiment at both $\mathbf{g}_\perp$ and $\mathbf{g}_\parallel$ (**Figure 4**). The measurement resulted in A = -13 and +10 at $\mathbf{g}_\parallel$ and A = -12 and -8 at $\mathbf{g}_\perp$. *Conditions:* 34.72 GHz, 100 ms repetition time, $\pi$ = 120 ns, $\tau$ = 600 ns, TRF = 15 μs, RF tail = 5 μs, 25 shots, 24 off.

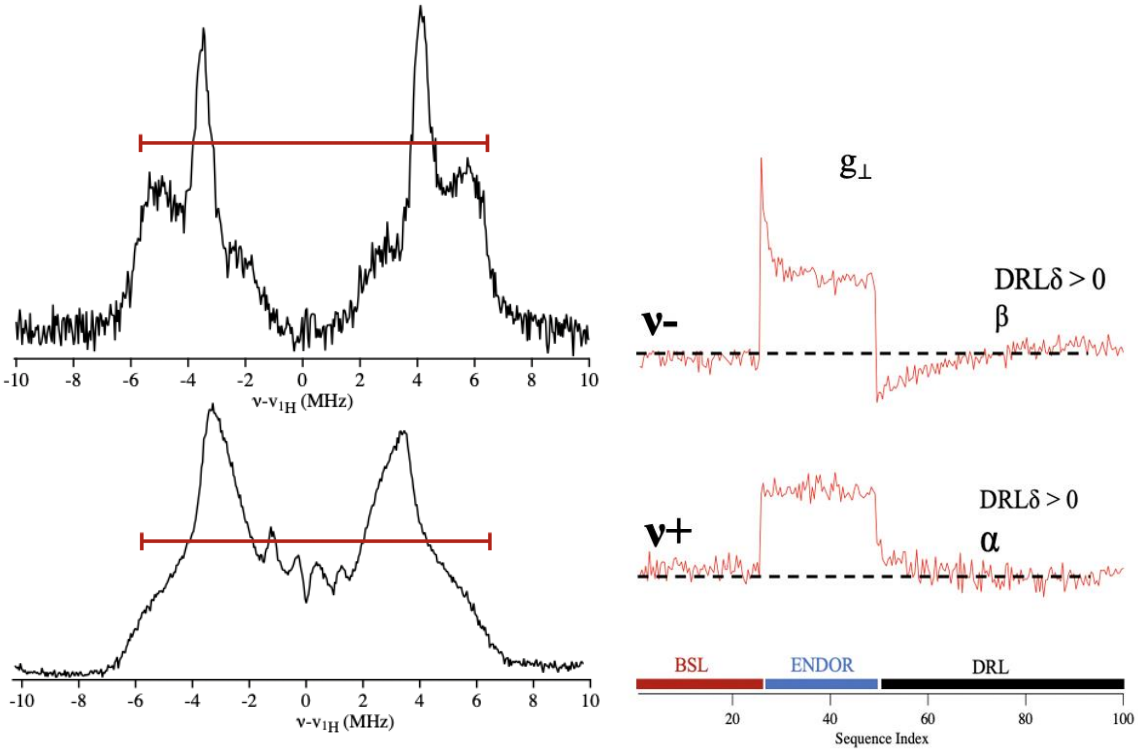


**Figure S7.** Q-band stochastic $^{1}$H ENDOR and PESTRE measurements of Cu(II)$(NH_3)_4$ in $H_2O$ buffer with ~20% ethylene glycol at $g_{\|}$ (10800G) (top) and $g_{\perp}$ (12020 G). Red brackets represent |A| for the largest $^{1}$H couplings, A ~ 12 MHz. Since $[Cu(II)(NH_3)_4]^{2+}$ does not contain axial ligands, the ~12 MHz $^{1}$H couplings at both $g_{\|}$ and $g_{\perp}$must come from the in-plane amine ligands. PESTRE measurements revealed the couplings at both g-values to be negative in sign. DFT model of $[Cu(II)(NH_3)_4]^{2+}$yields a hyperfine tensor, **A** = [-15, 1.5, -16] for an in-plane amine proton. This highly rhombic tensor is achieved due to large spin delocalization from the copper to the protons of the amine when they are oriented within the $x^2$-$y^2$ orbital of the unpaired electron. The tensor matches the signs and the identical relative magnitudes of those seen for the for the copper complex as well as for $Cu_B$.

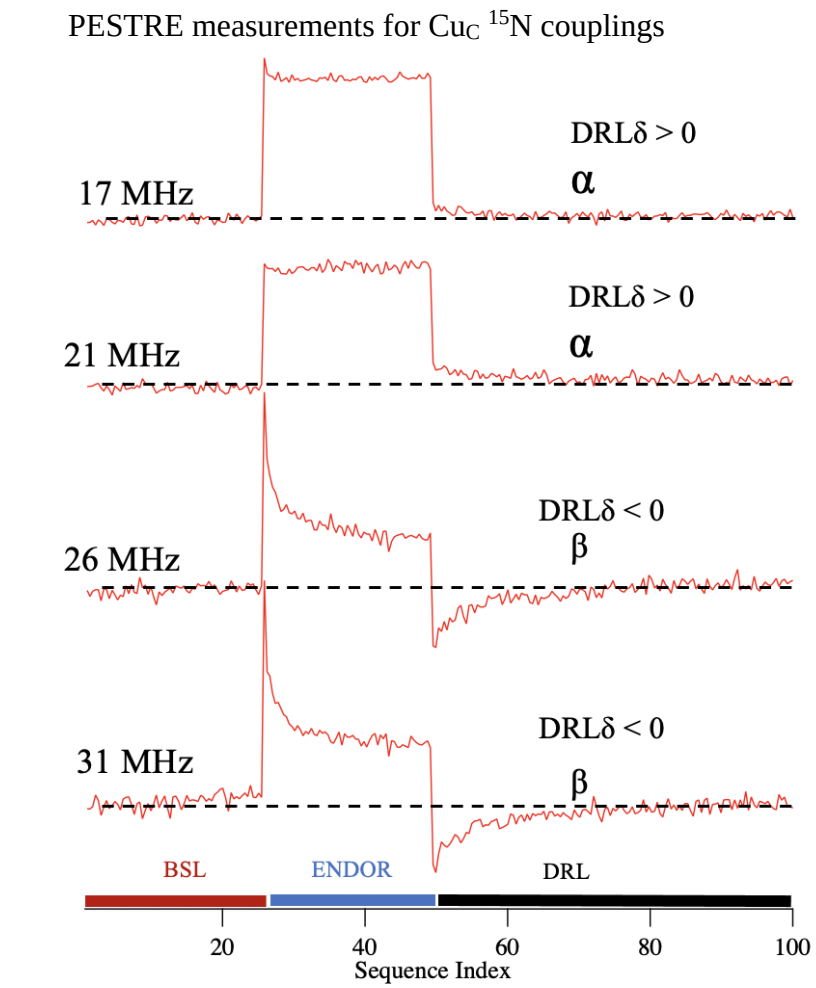


**Figure S8.** PESTRE measurements on Cu$_C$ $^{15}$N couplings at **g** = 2.33. The peaks examined at the frequency defined above are shown in **Figure 6**. The results of the PESTRE measurements reveal both strongly coupled $^{15}$N to the Cu$_C$ to be negative in sign. *Conditions:* 34.71 GHz, 100 ms repetition time, $\pi$ = 120 ns, $\tau$ = 600 ns, TRF = 15 μs, and RF tail = 5 μs. 25 shots, 24 off.

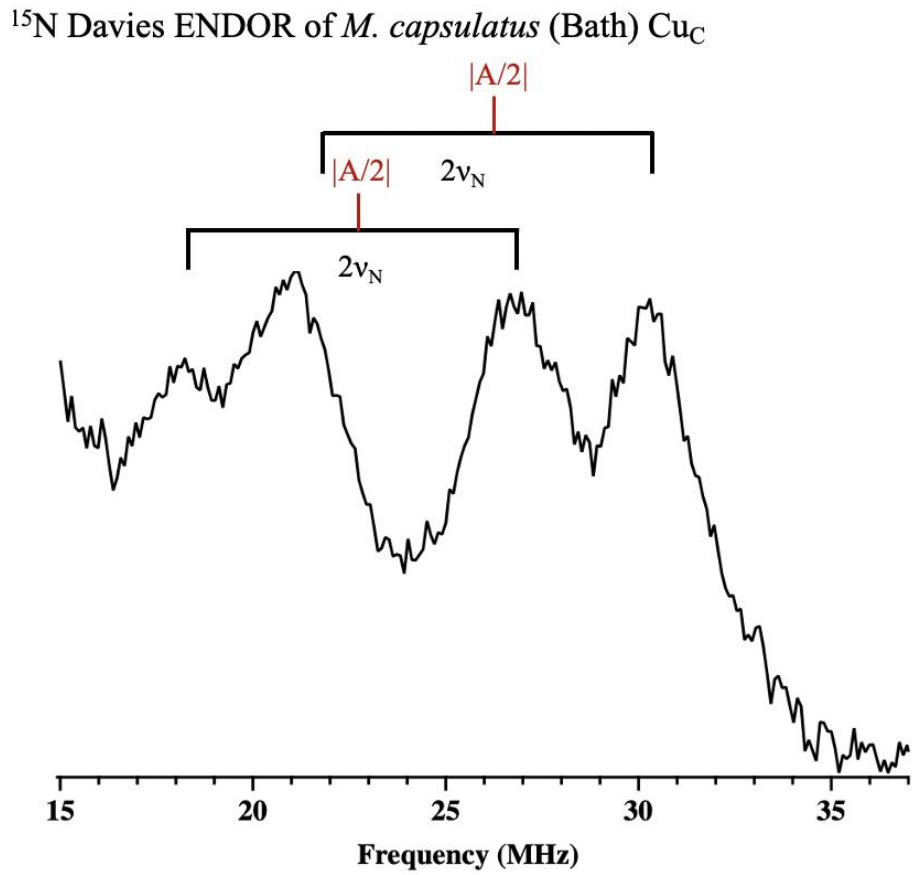


**Figure S9.** Medium Davies $^{15}$N ENDOR at a field of a corresponding g-value of g = 2.32 for $^{15}$N $^{63}$Cu *M. capsulatus* (Bath) pMMO. The $^{5}$N couplings observed here are exclusive to the $Cu_C$ site at this magnetic field and are identical in |A| to the type II *Mc.* sp. str. Rockwell pMMO, as shown in **Figure 6**, |A| ~ 50 MHz and |A| ~ 46 MHz. Brackets indicate twice the $^{15}$N Larmor frequency, and the center of the bracket (red) indicates |A/2|. *Conditions* are identical to **Figure 6** in the main text.

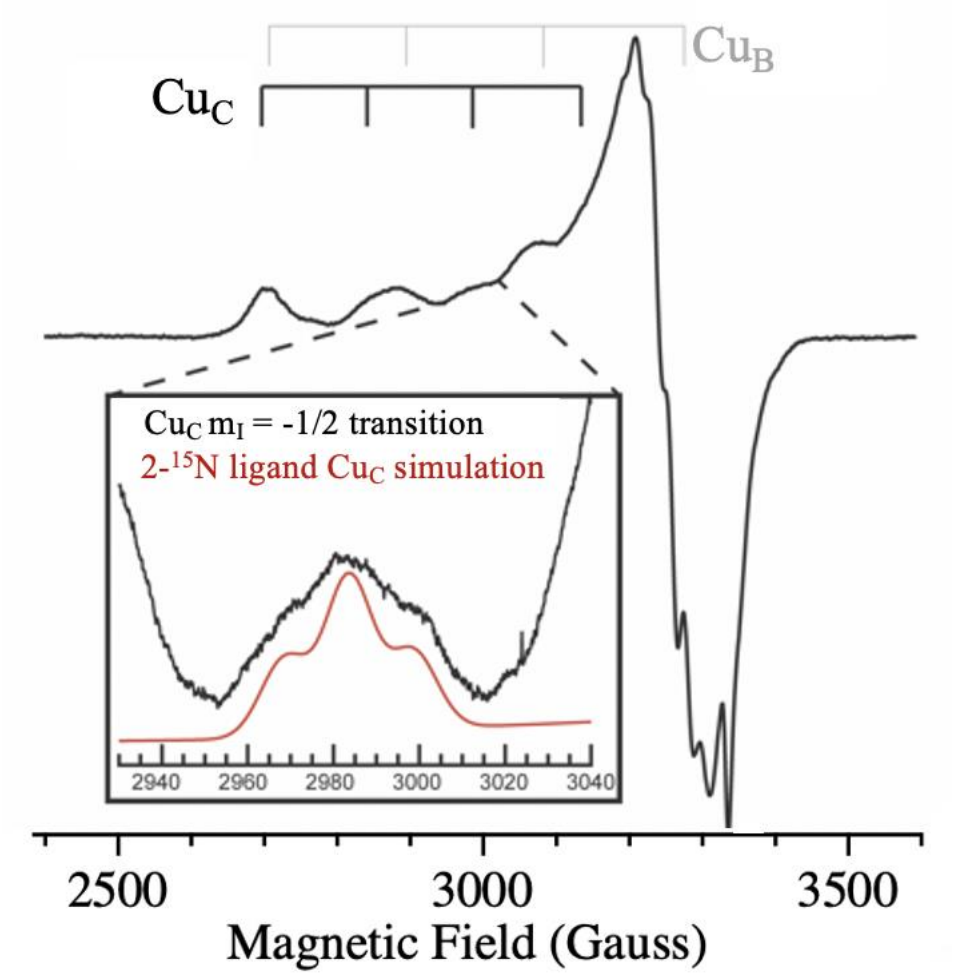


**Figure S10.** X-band CW EPR spectrum of the purified $^{15}$N, $^{63}$Cu-labeled *M. capsulatus* (Bath) pMMO in $D_2O$ and 10% $D_3$-glycerol exhibits overlapping $Cu_B$ and $Cu_C$ resonance. Brackets depict $^{63}$Cu $A_1$ hyperfine splitting attributable to the two Cu(II) centers. Inset depicts baseline-corrected narrow scans collected on the $g_{||}$ $Cu_C$ $m_I$ = -1/2 transition (black) and simulation of $Cu_C$ featuring two $^{15}$N ligands (red). *Conditions* for full spectrum: 9.365 GHz microwave frequency, 80 ms time constant, 10 G modulation amplitude, 90 s scan rate, temperature 180 K. *Conditions* for inset were the same except for a 60 s scan rate. *Simulation parameters*: **g** = [2.022, 2.068, 2.295], $^{63}$Cu $A_{||}$ = [-440] MHz, 2 isotropic $^{15}$N couplings $A_{iso}$ = -48 MHz, 13 G full width at half maximum isotropic linewidth.

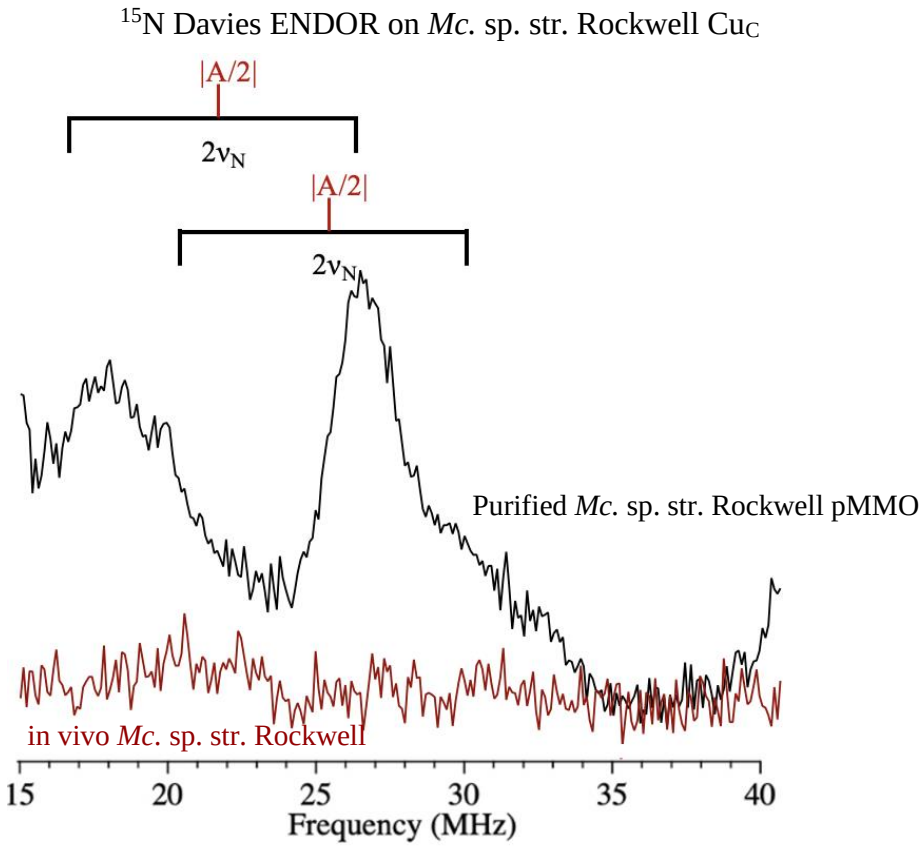


**Figure S11.** $^{15}$N Davies pulsed ENDOR of *Mc.* sp. str. Rockwell pMMO Cu$_C$ (black trace) site at the low-field end of the EPR signal, at a field with a corresponding g-value of g = 2.34, (~10600 G). The red trace is in vivo *Mc.* sp. str. Rockwell pMMO, which exhibits an EPR signal from Cu$_B$ only, at the same field position. The two spectra were echo-normalized. Brackets indicate twice the $^{15}$N Larmor frequency and the center of the bracket (red) indicates |A/2|. The larger coupling is not well resolved at this field. *Conditions* are identical to **Figure 6** in the main text.

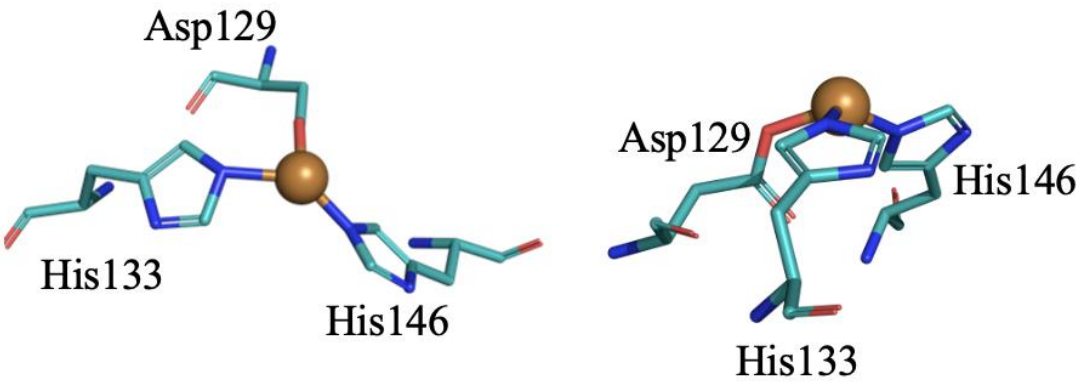


**Figure S12**. Alternative view of PmoC copper site from the crystal structure of *Mc*. sp. str. Rockwell (PDB accession code 4PHZ). The view shows the distortion (lack of symmetry) of the two His coordinating ligands to the copper center.

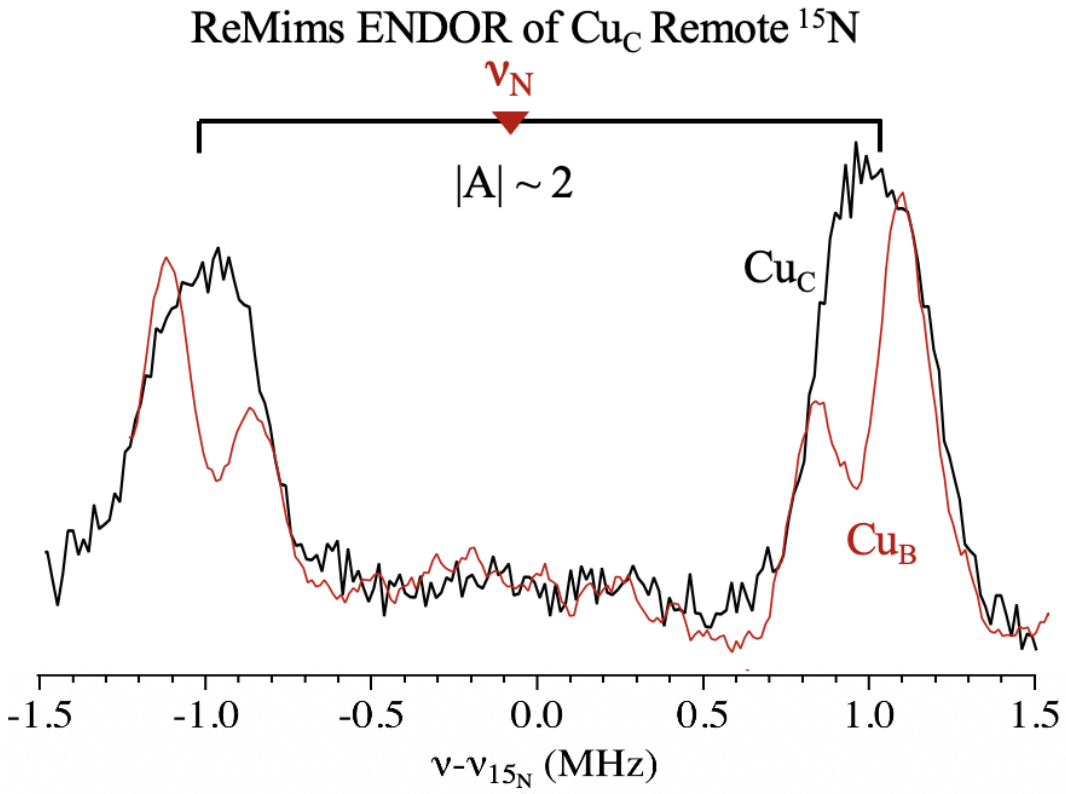


**Figure S13.** Overlay of ReMims ENDOR remote $^{15}$N couplings from the $Cu_B$ (red, from **Figure 2**) and $Cu_C$ (black, from **Figure 7**). Comparing the breadth of the unresolved doublet to the doublets in the $Cu_B$ spectrum reveal that the couplings in the $Cu_C$ spectrum likely arise from more than one remote $^{15}$N coupling as discussed in the text.

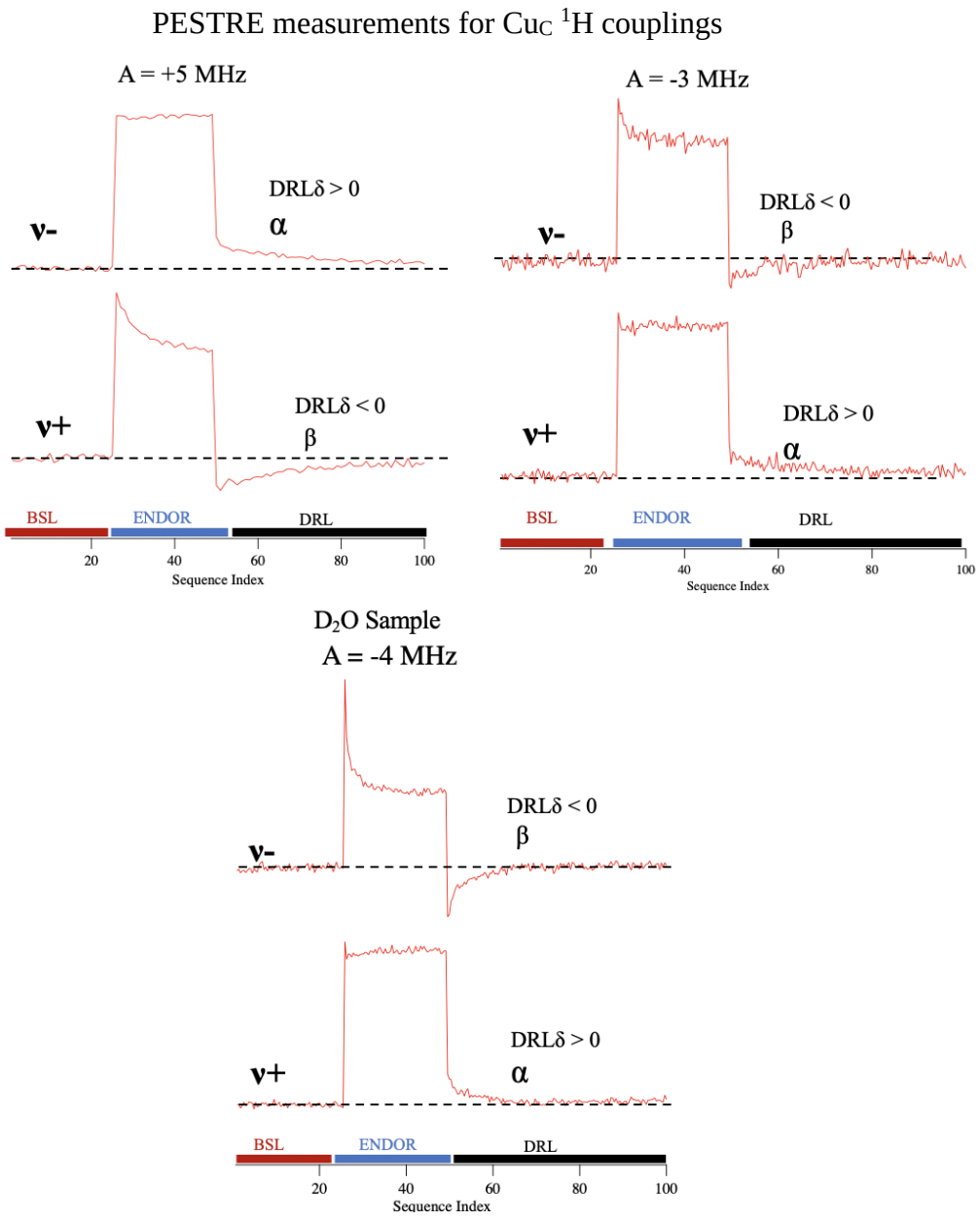


**Figure S14.** 35 GHz PESTRE performed on the $Cu_C$ $^1H$ couplings at g = 2.34 (10700G). The +5 MHz and -2.5 MHz couplings were determined using a purified sample in $H_2O$, while the -4 MHz coupling was determined using a purified *Mc.* sp. str. Rockwell pMMO sample exchanged into $D_2O$. *Conditions:* 34.67 – 34.69 GHz, 100 ms repetition time, $\pi$ = 120 ns, $\tau$ = 600 ns, TRF = 15 µs, and RF tail = 5 µs. 25 shots, 24 off.

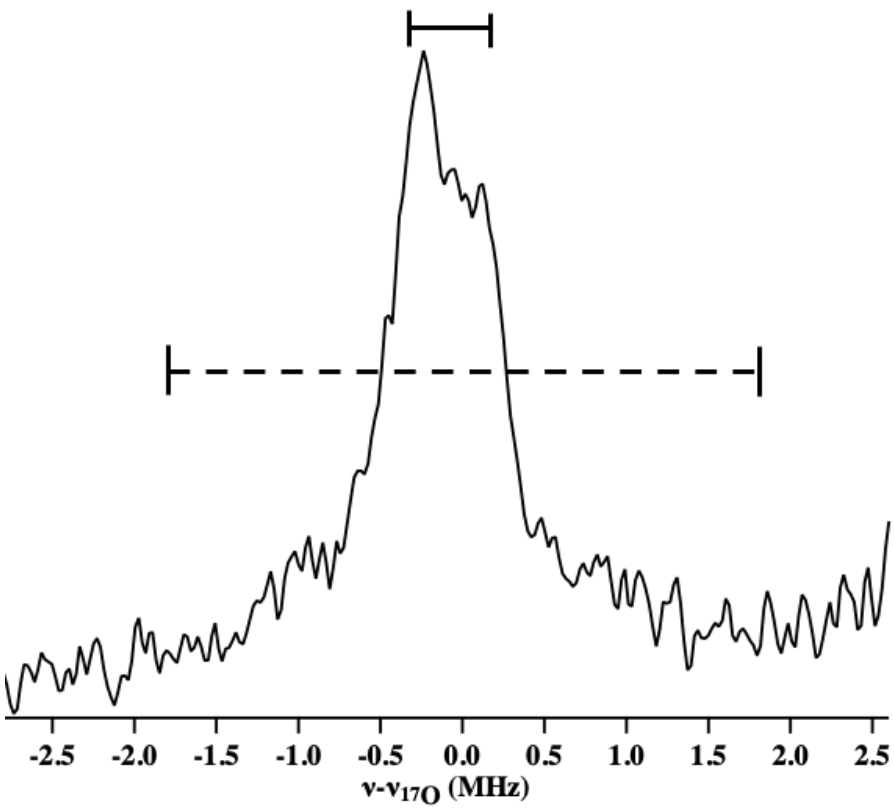


**Figure S15.** $^{17}$O ENDOR at g = 2.33 ($Cu_C$ site). The spectrum specifically lacks the ~3.6 MHz doublet (indicated by the dashed 'goalposts') previously reported observing at g = 2.01 for $Cu_C$. The spectrum instead exhibits a response centered at the Larmor frequency, which is expected for remote $H_2{}^{17}O$ solvent in the sample, and may exhibit unresolved intensity, breadth ~ 2 MHz, from a secondary coordination sphere water, whose $^1$H ENDOR response is discussed in Figure 8.

$^{17}$O Mims ENDOR on purified *M. capsulatus* (Bath) pMMO

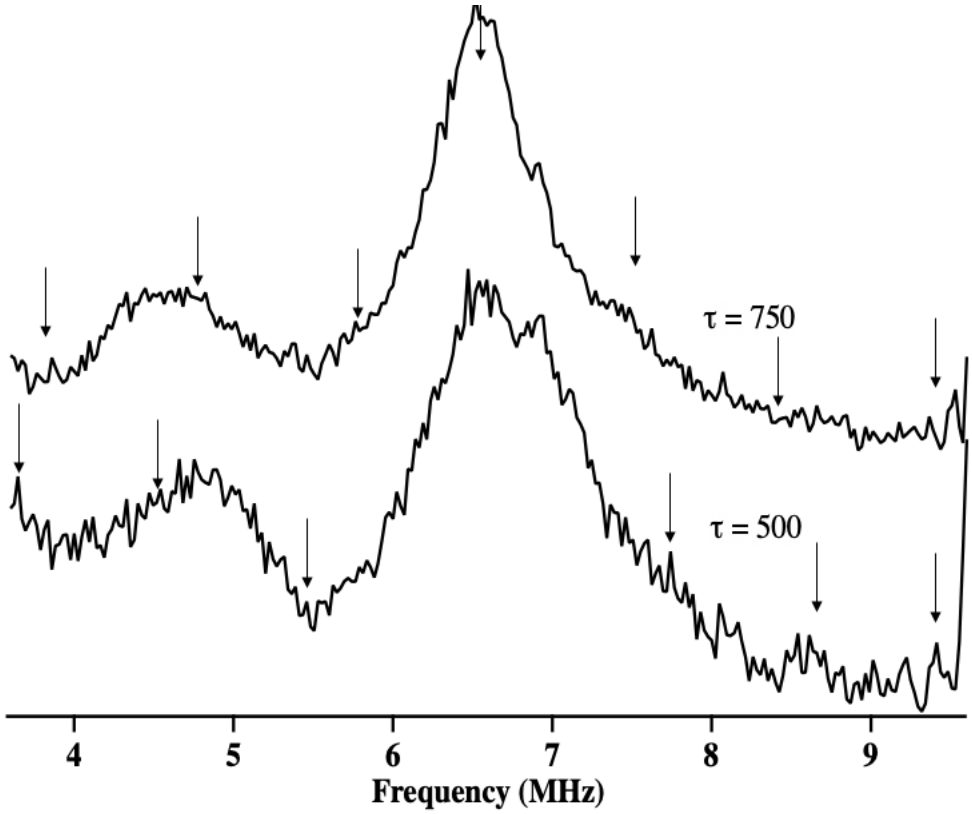


**Figure S16.** $^{17}$O Mims Pulsed ENDOR of purified *M.* capsulatus (Bath) pMMO in 45% enriched $H_2{}^{17}O$ buffer at g = 2.02 (~12050 G). This experiment was conducted at different τ values to observe whether there is suppression of the large coupling (3.5 MHz). The τ = 750 experiment should suppress the coupling, but it looks quite resolved here. The coupling is now believed to derive from either a weakly coupled $^{14}$N or 5/2 quadrupole of the $Cu_B$ axial $H_2O$ ligand.

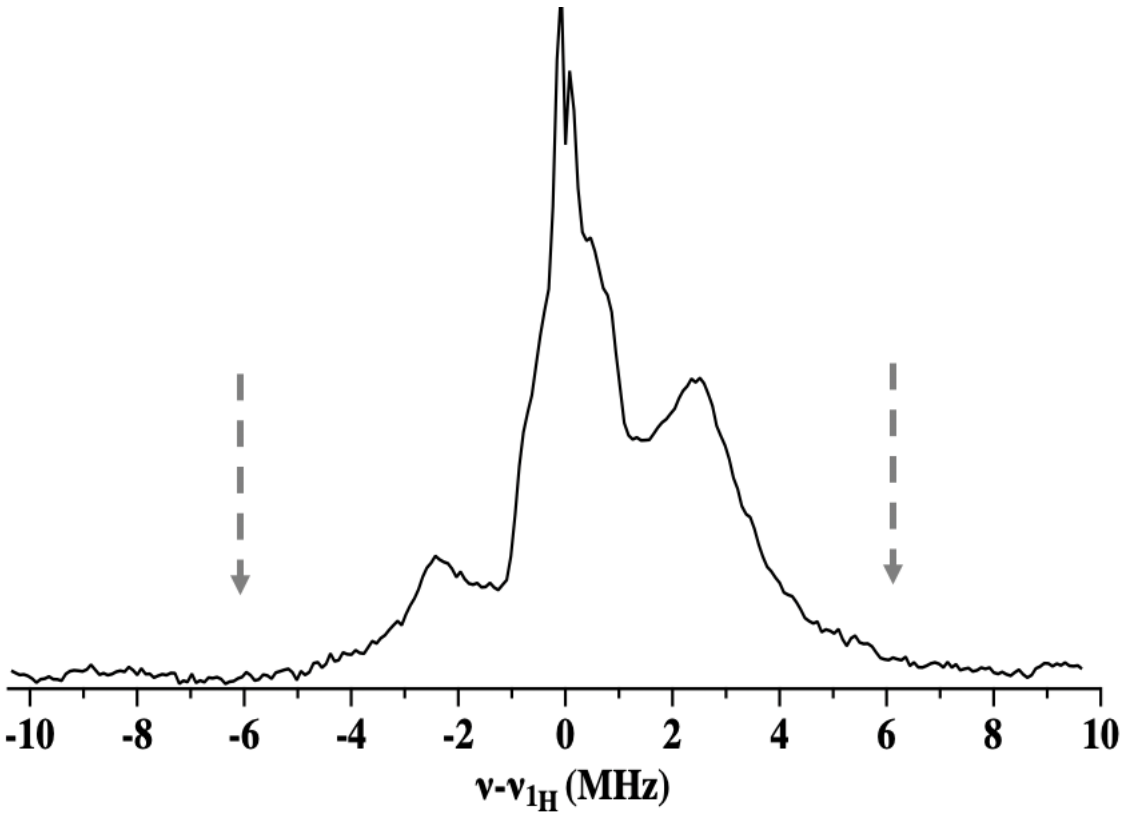


**Figure S17.** $^1$H CW ENDOR spectrum at g = 2.35 of *Mc.* sp. str. Rockwell purified pMMO $Cu_C$ site. The gray dashed arrows highlight the absence of any couplings with A >8 MHz, which signifies the absence of a bound axial solvent molecule. This also serves as an additional control that only the $Cu_C$ site is observed at this field position since the $Cu_B$ site exhibits couplings of ~12 MHz at $g_{\|}$.

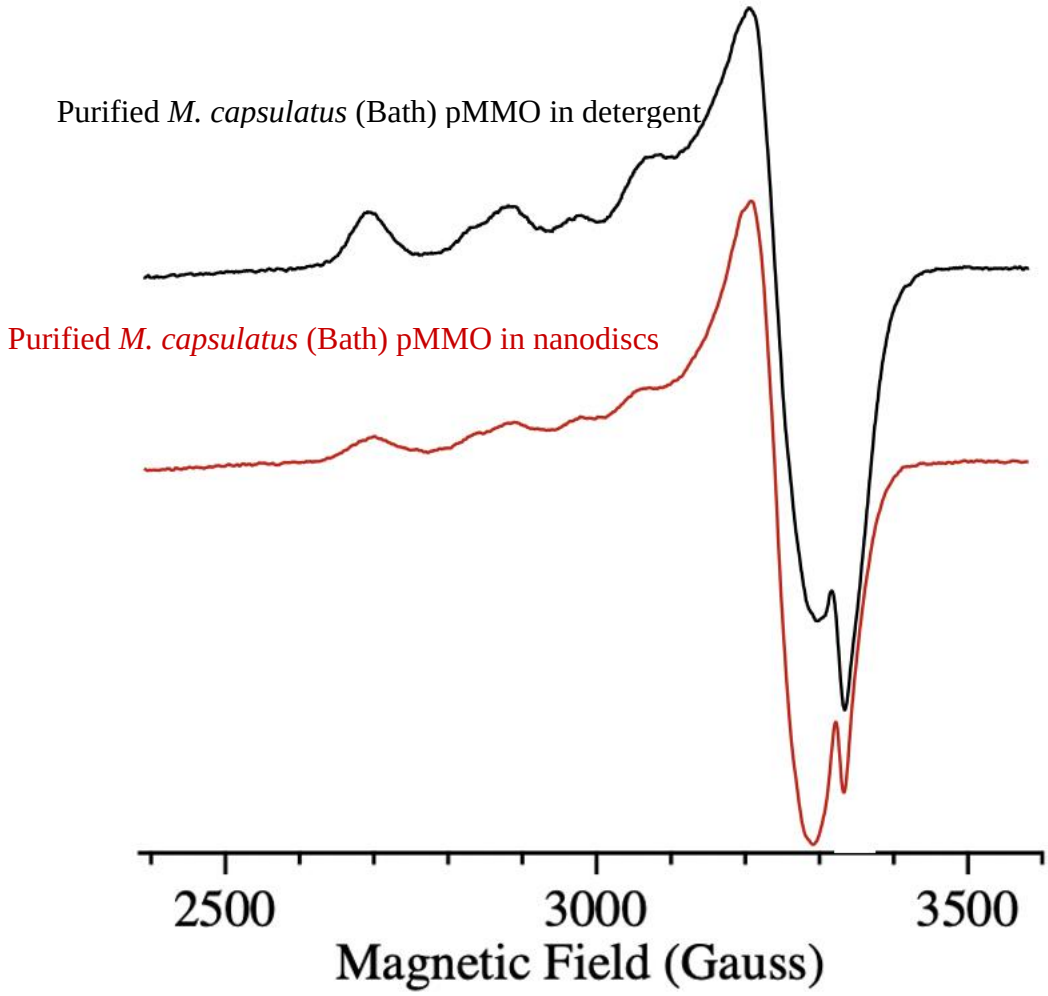


**Figure S18.** X-band EPR spectra of detergent-purified natural abundance *M.* capsulatus (Bath) pMMO (black) and purified *M.* capsulatus (Bath) pMMO in nanodiscs (red). The spectra are scaled by EPR intensity to facilitate comparison. The two sites exhibit identical g values and $^{63}$Cu A values. *Conditions:* 9.37 GHz MW Frequency, 30 K, 12.5 G modulation, 10 G/s sweep rate, 320 ms time constant, 200μW power.

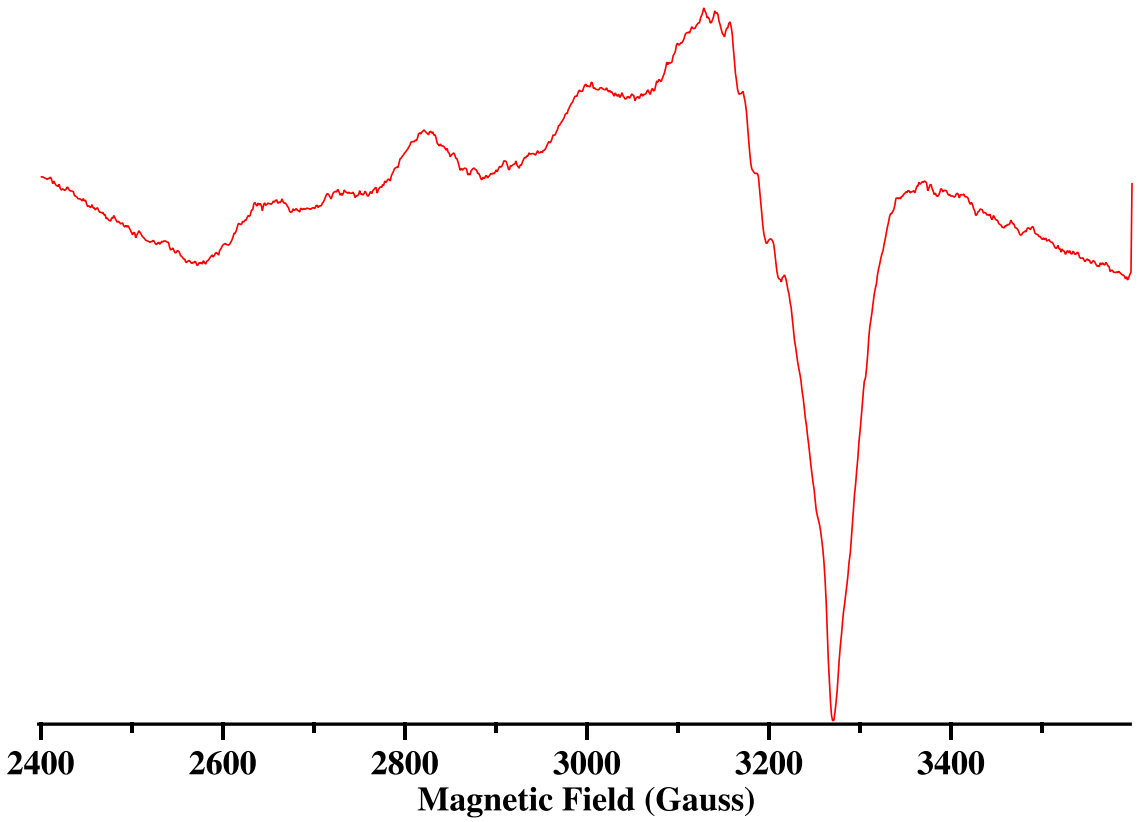


**Figure S19.** X-band EPR spectrum of reduced *M. capsulatus* (Bath) pMMO in nanodiscs. 12:1 ascorbic acid per 100 kDa protomer of pMMO was added to reduce the $Cu_C$ site and obtain a pure $Cu_B$ site to investigate with ENDOR. *Conditions:* 77K, 12.5 G modulation, 200μW MW power, 320 ms time constant, 9.37 GHz frequency. .

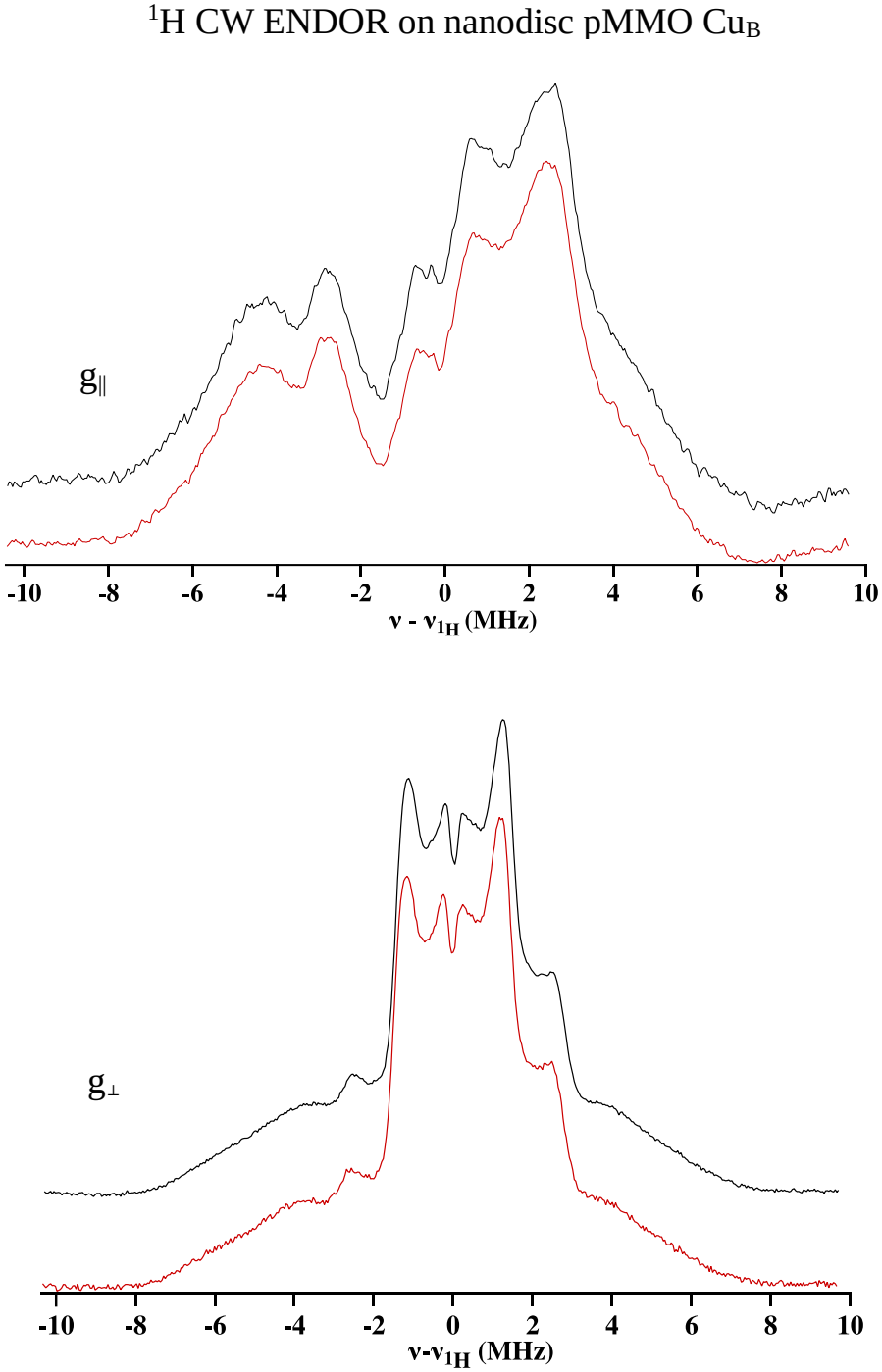


**Figure S20.** $^1$H CW ENDOR of $Cu_B$ in reduced purified *M. capsulatus* (Bath) pMMO in detergent (black trace) and in nanodiscs (red trace) at g‖ (top) and $g_{\perp}$ (bottom). The ENDOR spectra show no differences, indicating that $Cu_B$ is identical within the two different environments, unlike $Cu_C$ in which the secondary coordination sphere loses a solvent molecule (**Figure 9**). *Conditions:* 2K, 34.89 GHz MW frequency, 3.2 G modulation, 0.5 MHz/s scan rate, 30dB MW power, 13dB RF power, 32 ms time constant. Spectra were collected with RF swept low to high frequency.

**References**


(1) Neese, F., The ORCA program system. *WIREs Comput. Mol. Sci.* **2012,** *2*, 73-78.

(2) Hanwell, M. D.; Curtis, D. E.; Lonie, D. C.; Vandermeersch, T.; Zurek, E.; Hutchison, G. R., Avogadro: an advanced semantic chemical editor, visualization, and analysis platform. *J. Cheminformatics* **2012,** *4*, 17.

(3) Becke, A. D., Density-functional exchange-energy approximation with correct asympototic behavior. *Phys. Rev. A* **1988,** *38*, 3098-3100.

(4) Lee, C. T.; Yang, W. T.; Parr, R. G., Development of the Colle-Salvetti correlation-energy formula into a functional of the electron density. *Phys. Rev. B* **1988,** *37*, 785-789.

(5) Schäfer, A.; Huber, C.; Ahlrichs, R., Fully optimized contracted Gaussian basis sets of triple zeta valence quality for atoms Li to Kr. *J. Chem. Phys.* **1994,** *100*, 5829-5835.

(6) Barone, V., Structure, magnetic properties and reactivities of open-shell species from density functional and self-consistent hybrid methods. In *Recent advances in density functional methods*, Chong, D. P., Ed. World Scientific: Singapore, 1995; pp 287-334.

(7) Rega, N.; Cossi, M.; Barone, V., Development and validation of reliable quantum mechanical approaches for the study of free radicals in solution. *J. Chem. Phys.* **1996,** *105*, 11060-11067.

(8) Schindler, M.; Kutzelnigg, W., Theory of magnetic susceptibilities and NMR chemical shifts in terms of localized quantitites. II. Application to some simple molecules. *J. Chem. Phys.* **1982,** *76*, 1919-1933.

(9) Neese, F., Efficient and accurate approximations to the molecular spin-orbit coupling operator and their use in molecular g-tensor calculations. *J. Chem. Phys.* **2005,** *122*, 13.

(10) Smith, S. M.; Rawat, S.; Telser, J.; Hoffman, B. M.; Stemmler, T. L.; Rosenzweig, A. C., Crystal structure and characterization of particulate methane monooxygenase from *Methylocystis* species strain M. *Biochemistry* **2011,** *50*, 10231-10240.

(11) Hakemian, A. S.; Kondapalli, K. C.; Telser, J.; Hoffman, B. M.; Stemmler, T. L.; Rosenzweig, A. C., The metal centers of particulate methane monooxygenase from *Methylosinus trichosporium* OB3b. *Biochemistry* **2008,** *47*, 6793-6801.